The FASEB Journal article fj.09-141036. Published online July 20, 2010.

Enhanced cellular internalization and gene silencing with a series of cationic dendron-multiwalled carbon nanotube:siRNA complexes

Khuloud T. Al-Jamal,* Francesca M. Toma,[†] Açelya Yilmazer,* Hanene Ali-Boucetta,* Antonio Nunes,* Maria-Antonia Herrero,[†,‡] Bowen Tian,* Ayad Eddaoui,[§] Wafa' T. Al-Jamal,* Alberto Bianco,[¶,1] Maurizio Prato,[†,1] and Kostas Kostarelos*[,1]

*Nanomedicine Laboratory, Centre for Drug Delivery Research, School of Pharmacy, University of London, London, UK; [†]Center of Excellence for Nanostructured Materials, Department of Pharmaceutical Sciences, University of Trieste, Trieste, Italy; [‡]Departamento de Química Orgánica, Facultad de Química, Universidad de Castilla-La Mancha, Ciudad Real, Spain; [§]Flow Cytometry Core Facility, University College London, Institute of Child Health, London, UK; and [¶]Centre National de la Recherche Scientifique, Institut de Biologie Moléculaire et Cellulaire, UPR 9021 Immunologie et Chimie Thérapeutiques, Strasbourg, France

ABSTRACT **One of the major obstacles to the clinical development of gene silencing by small interfering RNA (siRNA) is its effective cytoplasmic delivery. Carbon nanotubes have been proposed as novel nanomaterials that can offer significant advantages for the intracellular delivery of nucleic acids, such as siRNA. We recently demonstrated in a proof-of-principle study that amino-functionalized multiwalled carbon nanotubes (*f*-MWNT) can effectively deliver *in vivo* an siRNA sequence, triggering cell apoptosis that results in human lung xenograft eradication and prolonged survival. In the present study, we demonstrate how a newly synthesized series of polycationic dendron-MWNT constructs with a precisely tailored number of amino functions (dendron generations) can complex and effectively deliver double-stranded siRNA to achieve gene silencing *in vitro*. A systematic comparison between the *f*-MWNT series in terms of cellular uptake, cytotoxicity, and siRNA complexation is offered. Significant improvement in siRNA delivery with the dendron-MWNT conjugates is shown, and gene silencing was obtained in 2 human cell lines using 2 different siRNA sequences. The study reveals that through *f*-MWNT structure-biological function analysis novel nanotube-based siRNA transfer vectors can be designed with minimal cytotoxicity and effective delivery and gene-silencing capabilities.—Al-Jamal, K. T., Toma, F. M., Yilmazer, A., Ali-Boucetta, H., Nunes, A., Herrero, M.-A., Tian, B., Eddaoui, A., Al-Jamal, W. T., Bianco, A., Prato, M., Kostarelos, K. Enhanced cellular internalization and gene silencing with a series of cationic dendron-multiwalled carbon nanotube:siRNA complexes. *FASEB J.* 24, 000–000 (2010). www.fasebj.org**

Key Words: RNA interference · gene transfer · knockdown · nanotechnology · nonviral

THE EMERGENCE OF CARBON nanotubes (CNTs) as advanced nanomaterials and in particular toward biomedical and biotechnological applications is of great interest (1–3). In terms of the biologically relevant features of CNTs, one of the most attractive properties described is the capacity to translocate cellular barriers (such as the plasma membrane) by mechanisms that are novel and seem to be reminiscent of a nanoneedle piercing the cells (4). Numerous laboratories (4–8) using various types of CNTs have now reported their cellular uptake by a wide range of cells. The solubilization of pristine nanotubes by means of different functionalization strategies allowed the development of a wide variety of single-walled CNTs (SWNTs) and multiwalled CNTs (MWNTs) that have shown promise in terms of biocompatibility and the ability to cross the plasma membrane and to act as transporters for drugs (9–13), biological molecules such as peptides and proteins (6, 14–17), small interfering RNA (siRNA; refs. 18, 20–23), and plasmid DNA (7, 24–27). Despite conflicting reports on the toxicity profile of CNTs, chemically functionalized CNTs compared with pristine CNTs have shown promise with significantly lower cytotoxicity profiles obtained (28).

One of the approaches used for CNT-assisted siRNA delivery involves the chemical conjugation of siRNA to SWNTs or the material used to coat them. Kam *et al.* (18) conjugated pDNA and siRNA to phospholipid-coated SWNTs *via* cleavable disulfide linkages and

[1] Correspondence: K.K., Nanomedicine Laboratory, Centre for Drug Delivery Research, The School of Pharmacy, University of London, London WC1N 1AX, UK. E-mail: kostas.kostarelos@pharmacy.ac.uk; A.B., CNRS, Institut de Biologie Moléculaire et Cellulaire, UPR 9021 Immunologie et Chimie Thérapeutiques, 67000 Strasbourg, France. E-mail: a.bianco@ibmc-cnrs.unistra.fr; M.P., Center of Excellence for Nanostructured Materials, Department of Pharmaceutical Sciences, University of Trieste, 34127 Trieste, Italy. E-mail: prato@units.it

doi: 10.1096/fj.09-141036

demonstrated efficient siRNA delivery *in vitro*. SWNTs were also coated by the same group with lipopolymers bearing amine-terminated polyethylene glycol, shown to be effective transporters of siRNA in human T and primary cell cultures (22). More recently, siRNA for TRPC3 gene knockdown was chemically conjugated *via* disulfide bonds to a SWNT coated with PEGylated phospholipids and was shown to be able to silence the TRPC3 gene in extracted mouse skeletal muscle cells *ex vivo* (21).

An alternative approach is the formation of noncovalent complexes between the negatively charged siRNA and chemically functionalized cationic CNTs. Krajcik *et al.* (20) complexed siRNA against ERK protein expression using a double-functionalized cationic CNT, resulting in ERK knockdown in primary cardiomyocyte cultures. Following a similar approach, Wang *et al.* (29) reported that ammonium-functionalized SWNTs could electrostatically bind siRNA against cyclin A2, leading to growth inhibition and apoptosis of a human erythroleukemic cell line (K526) *in vitro*. Zhang *et al.* (23) reported the delivery of telomerase reverse transcriptase (TERT) siRNA by complexation with a positively charged SWNT, resulting in down-regulation of TERT and subsequent inhibition of cell proliferation *in vitro* and tumor growth delay *in vivo*. Our laboratories (30) reported that ammonium-functionalized MWNTs (MWNT-NH_3^+) were more effective than cationic liposomes in intratumoral *in vivo* delivery of cytotoxic siRNA and reported the first tumor growth arrest and prolonged survival of MWNT-NH_3^+:siRNA-treated animals bearing a human lung cancer xenograft (Calu6).

One of the strategies proposed to further enhance the aqueous dispersibility of CNTs by maintaining their cationic character is through their surface modification by growth of dendritic molecules (31, 32). The number of cationic functional groups on the dendron-MWNT surface can grow exponentially, in a controlled, stepwise manner, without the need for repeated or higher degree of chemical grafting on the CNT backbone minimizing the structural defects introduced on the nanotube backbone by functionalization chemistries. We have very recently reported the synthesis and structural characterization of a series of cationic dendron-MWNT constructs and their capacity to deliver fluorescently labeled siRNA intracellularly (32).

In this study, we present the structure-biological function relationships exhibited by the dendron-CNT constructs of this newly synthesized series. A variety of biological functions among the dendron-MWNT series were studied, including cellular internalization, cytotoxicity, capacity to condense and deliver siRNA in the cytoplasm, and finally, efficiency of gene silencing. The biological effects of dendron alkylation and the increase in dendritic branching were revealed. The rational design of the dendron-CNT series correlated with the capacity to internalize and deliver siRNA inside the cell cytoplasm and led to efficient gene silencing in human cells.

MATERIALS AND METHODS

Materials

MWNTs were purchased from Nanostructured & Amorphous Materials (Houston, TX, USA; stock no. 1240XH, 95%, OD 20–30 nm). Chemicals and solvents for synthesis and horseradish perioxidase (HRP)-linked anti-mouse IgG were obtained from Sigma-Aldrich (St. Louis, MO, USA), and they were used as received. To achieve the synthesis of dendron functionalized carbon nanotubes, we followed the procedure reported in ref. 31. The proprietary sequence siCONTROL TOX (referred to throughout this work as siTOX) was purchased from Dharmacon (Lafayette, CO, USA). Noncoding siNEG and Atto 655-labeled siNEG were purchased from Eurogentec (Southampton, UK). The DeadEnd Fluorometric TUNEL system was from Promega (Southampton, UK). The annexin-V-Fluos staining kit was from Roche Diagnostics (Mannheim, Germany). DMEM, minimum essential medium (MEM), FBS, propidium iodide (PI), penicillin/streptomycin, and PBS were from Life Technologies, Inc. (Invitrogen, Paisley, UK). Citifluor reagent was from Citifluor (London, UK). Paraformaldehyde and RNase were from Sigma. The cervical cancer cell line HeLa (CCL-2.2) and human lung carcinoma A549 (CCL-185) were from American Type Culture Collection (ATCC; London, UK). The BCA protein assay kit, Restore Plus Western blot stripping buffer, and ECL detection system were purchased from Pierce (Rockford, IL, USA). Tropix Galactolight Plus lysis buffer was obtained from Applied Biosystems (Foster City, CA, USA). Silencer GFP (eGFP) siRNA (catalog no. Am4626), referred to through the study as siGFP, and mouse anti-GAPDH antibody were obtained from Ambion (Austin, TX, USA). Hybond ECL nitrocellulose membranes were obtained from GE Healthcare (Little Chalfont, UK). Rabbit polyclonal GFP antibody was obtained from Abcam (Cambridge, MA, USA). HRP-linked anti-rabbit IgG was obtained from Cell Signaling (Danvers, MA, USA). Recombinant adenovirus type-5 encoding enhanced green fluorescent protein (Ad-eGFP) was purchased from the Baylor College of Medicine Vector Development Laboratory (Houston, TX, USA).

Transmission electron microscopy (TEM)

A drop of the *f*-MWNT dispersion (0.5 mg/ml) was placed on a grid with a support film of Formvar/carbon, excess material was blotted off with a filter paper, and the complexes were examined under a FEI CM120 BioTwin transmission electron microscope (FEI Tecnai, Einhoven, Netherlands) using a Lab6 emitter. Images were captured using an AMT digital camera (Advanced Microscopy Techniques, Danvers, MA, USA). For TEM of the siRNA complexes with CNTs, MWNT-2.0-D-N$(CH_3)_3^+$,15 μl of 1.0 mg/ml in 10% dextrose was complexed with an equal volume of siRNA solution to achieve 1:8 or 1:16 siRNA:MWNT-2.0-D-N$(CH_3)_3^+$ mass ratio. The complex was left to equilibrate for 30 min before the TEM microscopy was performed.

Atomic force microscopy (AFM)

MWNT-2.0-D-N$(CH_3)_3^+$ (15 μl of 0.1 mg/ml in water) was complexed with an equal volume of siRNA at 1:8 and 1:16 siRNA:MWNT-2.0-D-N$(CH_3)_3^+$ mass ratios. The complexes were left to equilibrate for 30 min. Approximately 20 μl of siRNA, MWNT-2.0-D-N$(CH_3)_3^+$, or the complex was deposited on the surface of freshly cleaved mica (Agar Scientific, Essex, UK) and allowed to adsorb for 5 min. Unbound structures were removed by washing with 0.22 μm filtered

deionized H_2O, then dried under a nitrogen stream. Imaging was carried out in tapping mode using a Multimode AFM, E-type scanner, Nanoscope IV controller, Nanoscope 5.12b control software (Veeco, Cambridge, UK) and a silicon tapping tip, made of crystallized silicon (NSG01; NTI-Europe, Apeldoorn, The Netherlands) of curvature radius of 10 nm. The tip was mounted on tapping-mode silicon cantilever with a typical resonant frequency of 150 kHz and a force constant of 5.5 N/m to image 5- × 5-μm square areas of the mica surface, with a resolution of 512 × 512 pixels and a scan rate of 1 Hz. All AFM images were performed in air.

Cell culture

A549 cells and HeLa cells were maintained and passaged in DMEM or MEM, respectively, supplemented with 10% FBS, 50 U/ml penicillin, 50 μg/ml streptomycin, 1% L-glutamine, and 1% nonessential amino acids, at 37°C in 5% CO_2.

Cellular uptake studies of *f*-MWNTs by A549 cells

A549 cells were subcultured into 24-well plates (5×10^4 cells/well) for 24 h before incubation with the *f*-MWNTs. Cells were incubated with *f*-MWNT (0–40 μg/ml) in serum-free medium for 4 h, after which serum-containing medium was added to make the final concentration of serum to 10%. Cells were allowed to interact with the *f*-MWNTs for 15 min, 60 min, 4 h, 24 h, and 72 h, at 37°C in a humidified atmosphere (5% CO_2) incubator. Monolayers were photographed before trypsinization to compare the results obtained from light microscopy with sideward scattering light analysis. For light scatter analysis by flow cytometry, cells were washed with PBS to remove unbound CNTs, trypsinized, centrifuged at 1000 rpm for 5 min at 4°C, resuspended in PBS, and then transferred to 1.5-ml microcentrifuge tubes and kept on ice for immediate analysis by flow cytometry.

Sideward scattering analysis of A549 cells by flow cytometry

Bivariate and univariate scatter histograms were set using the CyAn ADP Flow Cytometer (Beckman Coulter, Brea, CA, USA) equipped with Summit 4.3 software (Beckman Coulter). In the bivariate scatter histograms, the sideward scattering (SSC Lin, ordinate) *vs.* forward scattering histogram (FSC Lin, abscissa) was obtained. The forward scatter and side scatter detectors voltage had to be set in a way that both the negative control (a sample containing cells without CNT) and the positive control cells [a sample containing cells incubated with MWNT-2.0-D-N$(CH_3)_3^+$ for 24 h] could be visualized inside the scatter dot plot. The population containing cells only was selected to include all the cells being studied and exclude any cell debris. In order not to include the *f*-MWNTs in the cell population group, a suspension containing the highest concentration of *f*-MWNTs without any cells was run first to exclude any free CNT from the cell population.

The univariate histograms of cell number (counts, ordinate) *vs.* sideward scattering intensity (SSC Lin, abscissa) were plotted and gated for the cell population. The median sideward scattering intensity values (SSC Lin) were recorded and used for comparison. Data were expressed as fold changes in median sideward scattering intensity for a given *f*-MWNT-treated cell sample as compared with that of control cells.

Cell viability assays

A549 or HeLa cells were incubated with *f*-MWNTs in serum-free medium for 4 h, after which serum-containing medium was added to make the final concentration of serum to 10%. Toxicity was assessed after 24 or 48 h by one of the following cytotoxicity assays:

Annexin-V-FITC/PI staining

The assay was performed with an annexin-V-FITC/PI staining kit (Roche Diagnostics) according to the instructions of the manufacturer. In brief, after the pellets were harvested, cells were washed twice with PBS, resuspended into a single-cell suspension, and stained according to the manufacturer's instructions. Samples were analyzed on a flow cytometer using 488-nm excitation and a 530/40-nm band-pass filter for fluorescein detection and a filter 613/20 nm for PI detection. Electronic compensation of the instrument was performed to exclude overlapping of the 2 emission spectra. Cell death was expressed as percentage cell population stained with annexin V or with PI staining. A CyAn ADP flow cytometer (Beckman Coulter) was used to analyze 2×10^5 cells/sample.

TUNEL labeling

For detection of apoptosis, the DeadEnd Fluorometric TUNEL system was used to label nicked DNA through incorporation of fluorescein-12-dUTP. Samples were incubated with recombinant terminal deoxynucleotidyl transferase (rTdT) as per manufacturer's instructions, and fluorescein labeling was visualized using confocal laser scanning microscopy (CLSM; Zeiss LSM 510 Meta; Carl Zeiss, Oberkochen, Germany) using 30-mW 488-nm argon laser excitation source, LP 505-nm output filter, and a Plan-Neofluar ×10 lens. PI was used to counterstain nuclei.

Electrophoretic mobility shift assay

Then, 0.5 μg of siRNA in 30 μl of 5% dextrose complexed to *f*-MWNTs at different mass ratios (1:0 to 1:60 mass ratio) or 0.5 μg of free siRNA as a control was added to 1% agarose gel containing ethidium bromide. The gel was run for 45 min at 70 V and then photographed under ultraviolet light using the GeneGenius system (PerkinElmer Life and Analytical Sciences, Wellesley, MA, USA).

Evaluation of fluorescent siRNA complex uptake in HeLa cells

Atto 655-labeled siRNA (λ_{exc}=665 and λ_{em}=690 nm) was used to prepare fluorescent siRNA complexes to assess the ability of *f*-MWNTs to transfer siRNA into HeLa cells. siRNA was complexed with *f*-MWNTs at 1:16 mass ratio or with DOTAP:cholesterol cationic liposomes (2:1 M ratio) at 1:4 −/+ charge ratio. HeLa cells were grown to confluency on glass coverslips in 24-well tissue culture dishes at a density of 5×10^4 cells/well. Twenty-four hours later, cells were incubated with the fluorescent complexes. Briefly, 50 μl of the preformed siRNA complex was diluted 10 times with serum-free medium, yielding a final siRNA concentration of 80 nM (1 μg/ml). Four hours later, 150 μl of fresh medium containing 20% FBS was added to each well. After 4 and 24 h, cells were washed with PBS solution and fixed with 4% paraformaldehyde in PBS for 15 min at room temperature and then rinsed with PBS. For nuclear staining, cells were permeabilized with 0.1% Triton X-100 in PBS for 10 min at room temperature, RNase treated (100 μg/ml) for 20 min at 37°C, and incubated with PI (1 μg/ml) in PBS for 5 min then rinsed 3 times with PBS. Coverslips were mounted with aqueous poly vinyl alcohol

Citifluor reagent mixed with AF100 antifade reagent (10:1) before use. Slides were examined under the CLSM using ×63 oil immersion lens and using identical settings for each confocal study.

Silencing with dendron-MWNT:siGFP in Ad-GFP transfected A549 cells

A549 cells (2×10^4 cells/well) were seeded onto 24-well plates. Twenty-four hours later, cells were transfected with siGFP complexed with MWNT-2.0-D-N$(CH_3)_3^+$ at 1:8 or 1:16 mass ratio. Briefly, 100 μl of the preformed siGFP complexes was added to each well containing 400 μl of serum-free medium to achieve a final siGFP concentration of 52 nM. DOTAP (2 mM):Chol (1 mM) liposomes complexed with siGFP, at 1:4 −/+ charge ratio, were used as control. Four hours later, 500 μl of fresh medium containing 20% FBS was added to each well. After 14 h of incubation with the complexes at 37°C and 5% CO_2, cells were washed with PBS and 1 ml of serum-free medium containing Ad-GFP (10^8 particles/ml) was added into the wells. Three hours later, medium was replaced with fresh complete medium, and cells were incubated at 37°C in 5% CO_2. After 24 h, cells were lysed with Tropix Galactolight Plus lysis buffer, and lysates were centrifuged for 10 min at 13,000 rpm. Total protein concentration was assessed with the BCA protein assay kit, and 100 μg protein was taken from each supernatant and resolved on 12% SDS-PAGE gels and transferred to Hybond ECL nitrocellulose membranes. After blocking in 5% nonfat dry milk overnight, the blots were incubated with rabbit polyclonal GFP antibody at 1:5000 dilution. HRP-linked anti-rabbit IgG at 1:1000 dilution was used as secondary antibody. The specific bands were detected with ECL detection system. To get GAPDH-specific control bands, the blots were stripped with Restore Plus Western blot stripping buffer and reprobed with mouse anti-GAPDH antibody at 1:4000 dilution and then with HRP-linked anti-mouse IgG.

Transfection of HeLa Cells with siTOX

HeLa cells were subcultured (5000 cells/well) into 16-well chamber slides. Twenty-four hours later, cells were transfected with siTOX, an apoptosis-inducing siTOX. Briefly, 30 μl of the preformed *f*-MWNT:siTOX complex was diluted 5 times with serum-free medium, and 150 μl of the complex-containing medium was added to each well, yielding a final siTOX concentration of 80 nM. Four hours later, 150 μl of fresh medium containing 20% FBS was added to each well. Transfection efficiency (apoptosis) was assessed by TUNEL labeling after 24 and 48 h.

Statistical analysis

All conditions in 3 assays were tested in triplicate. Data are expressed as means ± SD where indicated. Statistical differences were analyzed using the Student's *t* test, and values of $P < 0.05$ were taken to be statistically significant.

RESULTS

The biological function of the tetra-alkylated ammonium-MWNT [MWNT-N$(CH_3)_3^+$] and the series of dendron-MWNT, first generation dendron-MWNT [MWNT-1.0-D-N$(CH_3)_3^+$] and second generation dendron-MWNT [MWNT-2.0-D-N$(CH_3)_3^+$] previously synthesized (**Fig. 1*A***) (32) was investigated. The ammonium-functionalized MWNT (MWNT-NH_3^+), which has been mostly explored for biological applications previously (4, 30, 33), was also included throughout these studies for comparison. Although MWNT-NH_3^+ is adequately dispersed in aqueous buffers, TEM imaging can reveal some degree of bundling and aggregation (Fig. 1*B*). Alkylation of the ammonium group [MWNT-N$(CH_3)_3^+$] improved the dispersibility and reduced bundling. Divergent synthesis of the first and second generation dendrons on MWNT-NH_3^+ followed by complete alkylation of the ammonium distal groups [MWNT-1.0-D-N$(CH_3)_3^+$ and MWNT-2.0-D-N$(CH_3)_3^+$] further improved the dispersibility of the nanotubes in aqueous phases. MWNT-2.0-D-N$(CH_3)_3^+$ in particular, resulted in dramatically improved dispersibility despite the relatively low amount of alkylated groups on the nanotube surface (Fig. 1*B*; $f = 0.212$ mmol/g). These data suggested that increasing the cationic character by alkylation and grafting of the dendrons on the MWNT surface correlated with improved aqueous dispersibility of the material.

To study the uptake of these *f*-MWNTs in human lung epithelial (A549) monolayers, nanotubes were incubated with the cells for 8 and 24 h at 10 μg/ml, and cells were examined by light microscopy, as shown in **Fig. 2**. Even though magnification in optical microscopy was low, a qualitative indication of the interactions can be obtained based on the amount of dark signal (from the nanotubes) and its association with cells. MWNT-NH_3^+ (Fig. 2*B*) interacted with cells; however, the alkylated [MWNT-N$(CH_3)_3^+$] and the dendron-functionalized constructs seemed to associate more with the cells. Similar observations were obtained with a different human cervical carcinoma (HeLa) using confocal microscopy and higher magnification (Supplemental Fig. S1). After 48 h, the dendron-MWNT constructs seemed to have translocated in the cytoplasm and the perinuclear region, similar to previous reports for *f*-MWNT and *f*-SWNT (34).

The increase in the sideward scattering of cells incubated with *f*-MWNT using a flow cytometry-based assay has been previously reported and was shown to be a reliable technique to assess interactions of CNTs with cells (35). As the nanotubes bound and internalized into cells, the granularity of the cells increased, which concomitantly increased the sideward scattering intensity. Representative results from light-scattering analysis are shown in **Fig. 3*A***. The 2-D dot plot of the forward scatter (FS Lin on the abscissa) and sideward scatter (SS Lin on the ordinate) of light by cells indicated that events with high forward scatter correspond to healthy cells, whereas events with low forward scatter correspond to cell debris (see control with dead cells). We investigated the role of parameters in the CNT-cell interactions: the increase in the degree of dendritic branching (*i.e.*, dendron generation; Fig. 3*B*), the dose

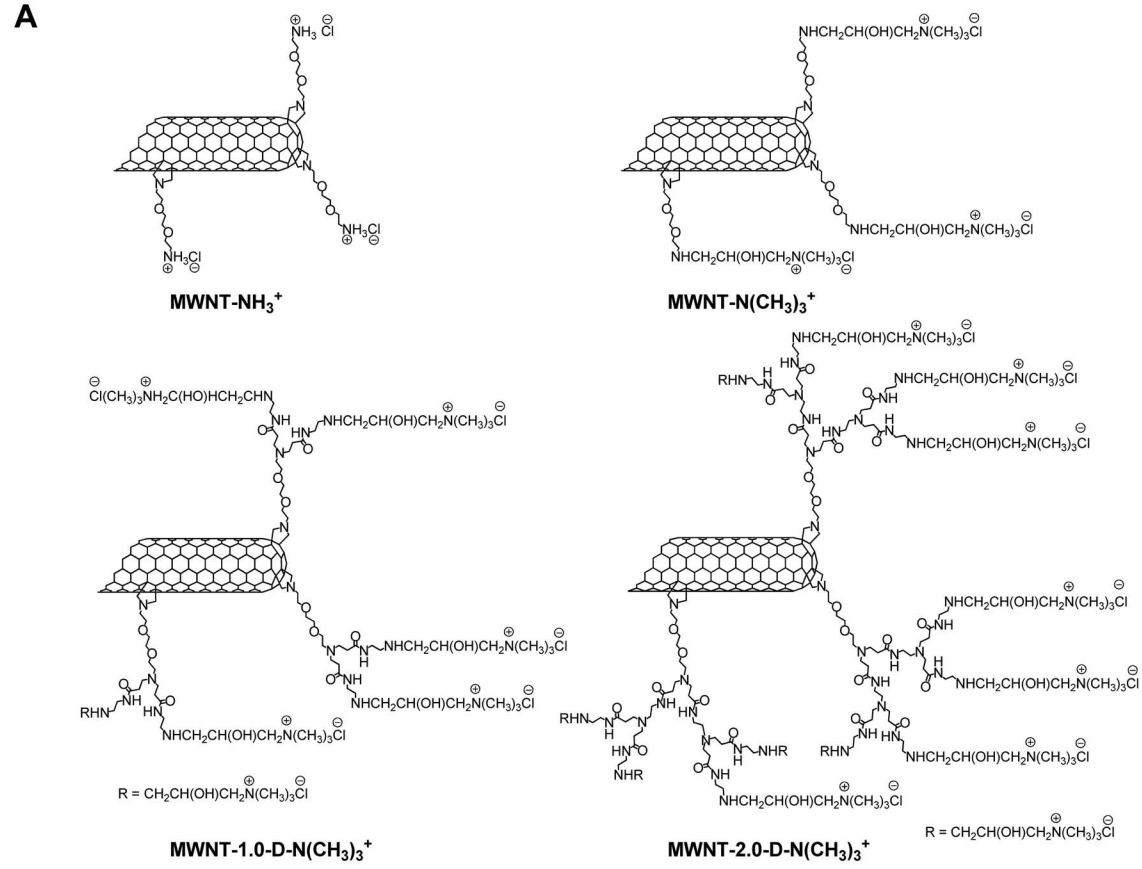

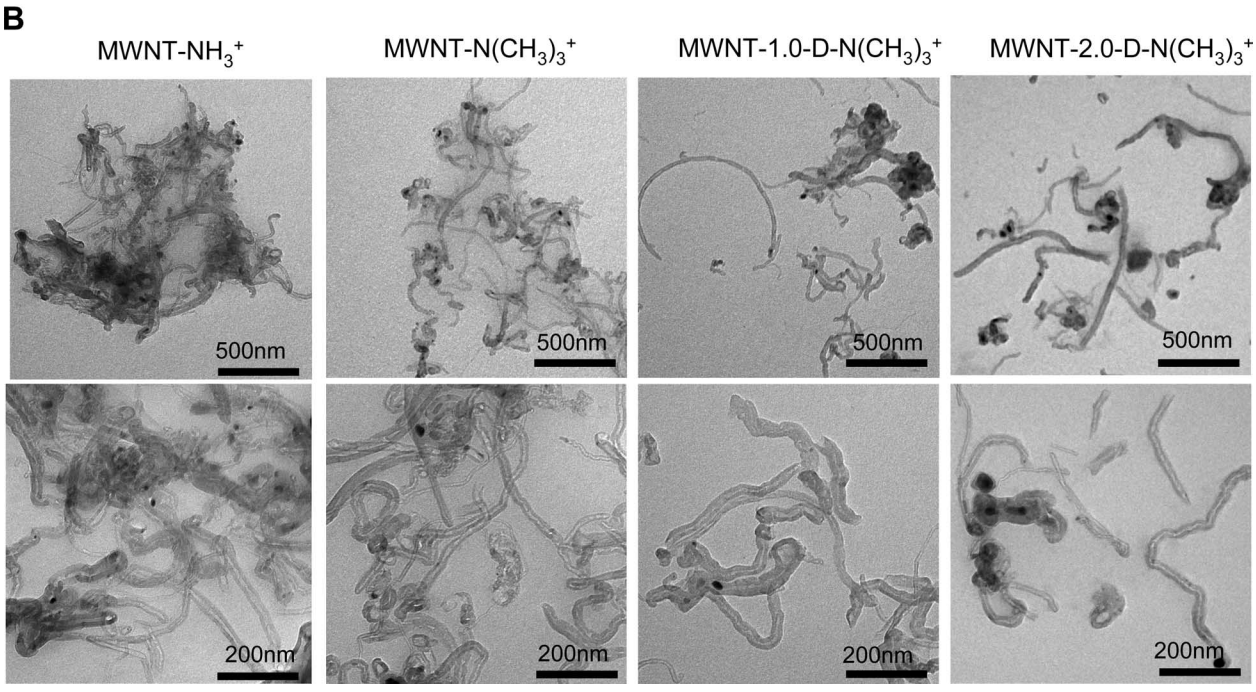

Figure 1. *A*) Molecular structures of *f*-MWNTs. Conjugate MWNT-NH_3^+ is the precursor of the different generations of alkylated dendron-MWNTs MWNT-$N(CH_3)_3^+$, MWNT-1.0-D-$N(CH_3)_3^+$, and MWNT-2.0-D-$N(CH_3)_3^+$. *B*) TEM of *f*-MWNT aqueous dispersions. TEM images of *f*-MWNTs at 250 μg/ml final concentration showing an increase in the dispersibility and individualization of *f*-MWNT following the alkylation of the amino groups by growing the dendritic branching.

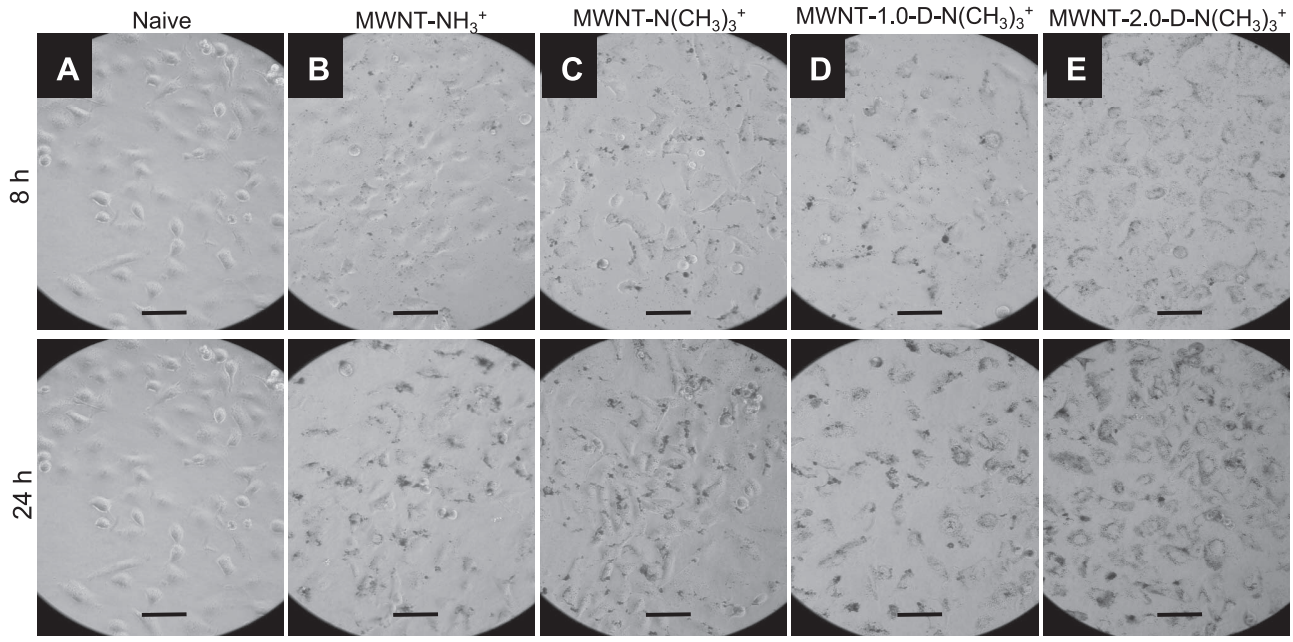

Figure 2. Cellular uptake of *f*-MWNTs by optical microscopy. Photomicrographs of A549 cells incubated with medium alone (control; *A*) or medium containing 10 μg/ml of MWNT-NH_3^+ (*B*), MWNT-$N(CH_3)_3^+$ (*C*), MWNT-1.0-D-$N(CH_3)_3^+$ (*D*), and MWNT-2.0-D-$N(CH_3)_3^+$ (*E*) for 8 or 24 h (×20). Cells were incubated with *f*-MWNTs in serum-free medium for 4 h, after which serum-containing medium was added to make the final concentration of serum to 10%. Uptake of *f*-MWNTs into cells was enhanced by increasing the incubation time (24 h>8 h, *A–E*), by increasing alkylation (*C*>*B*), and by increasing degree of dendritic branching (*E*>*D*>*C*). Scale bar = 20 μm.

(Fig. 3*C*), and the duration of interaction (Fig. 3*D*). The SS Lin median from the sideward scattering histogram was plotted and data analysis was carried out by calculating the increase in SS Lin of cells incubated with *f*-MWNTs as a percentage of control (cells alone; Fig. 3*B*, *E*). Cellular internalization was observed after incubation with MWNT-NH_3^+ and increased by 78% for the alkylated construct, while for the MWNT-1.0-D-$N(CH_3)_3^+$ and MWNT-2.0-D-$N(CH_3)_3^+$, increases of 100 and 140%, respectively, were obtained (Fig. 3*B*). These results were in agreement with the optical microscopy observations in Fig. 2 and indicated that MWNT-2.0-D-$N(CH_3)_3^+$ conjugates followed a concentration-dependent shift in the SS due to increases in cellular uptake (*i.e.*, granularity) from concentrations as low as 2.5 μg/ml. This shift was also time dependent, and maximum SS shift occurred after 24 h of incubation (Fig. 3*C*).

Although internalization of *f*-CNT into various types of cells can be seen as an attractive feature, there may be cytotoxic side-effects associated with such capacity that should be considered (36, 37). Since the light-scattering analysis of cells carried out above is not specific for either apoptosis or necrosis, the flow cytometric assay by staining with annexin V/PI was used for the determination of apoptosis or necrosis induced by the *f*-MWNT internalization. Freeze-thawed cells and untreated cells were used as positive (dead cells) and negative (healthy cells) controls. The percentage cell population stained is shown in **Fig. 4*A*, *B***, indicating that all *f*-MWNT constructs exhibited no significant toxicity to human lung carcinoma A549 cells (annexin V-negative and PI-negative cells) at a concentration of 10 μg/ml when compared with control cells after 24 h of incubation. Since MWNT-2.0-D-$N(CH_3)_3^+$ showed the highest cell internalization after 24 h by optical microscopy (Fig. 2*E*) and scattering analysis (Fig. 3*B*), we decided to escalate the concentration of MWNT-2.0-D-$N(CH_3)_3^+$ to determine whether higher doses could be tolerated. It was found that doses as high as 80 μg/ml (maximum tested) were well tolerated by the cells, with insignificant effects on cell viability after 24 h of incubation.

We further verified these cytotoxicity observations in HeLa cells and with the use of TUNEL labeling assay. The TUNEL reaction stains apoptotic cells, which appear green. Nuclei were counterstained using PI (in red). Cells treated with all 4 *f*-MWNT constructs exhibited no sign of apoptosis after 24 h interaction with up to 64 μg/ml *f*-MWNTs (Fig. 4*C*). Interestingly, all alkylated *f*-MWNTs (not the MWNT-NH_3^+) were found toxic to HeLa cells after 48 h incubation at 32 and 64 μg/ml (Fig. 4*D*). Based on the above, we determined that in order to avoid any unwanted cytotoxic side-effects further studies would be carried out using a maximum incubation period with cells of 24 h.

It has been previously shown that cationic *f*-CNTs were able to condense nucleic acids efficiently and deliver them into mammalian cells (26, 27, 30). Complexation of siRNA with the series of dendron-MWNTs was determined by agarose gel electrophoresis **(Fig. 5*A*)**. The amount of free (uncomplexed) siRNA migrating into the gel was reduced on complexation, most noticeable in the case of MWNT-2.0-D-$N(CH_3)_3^+$ at 60:1 mass

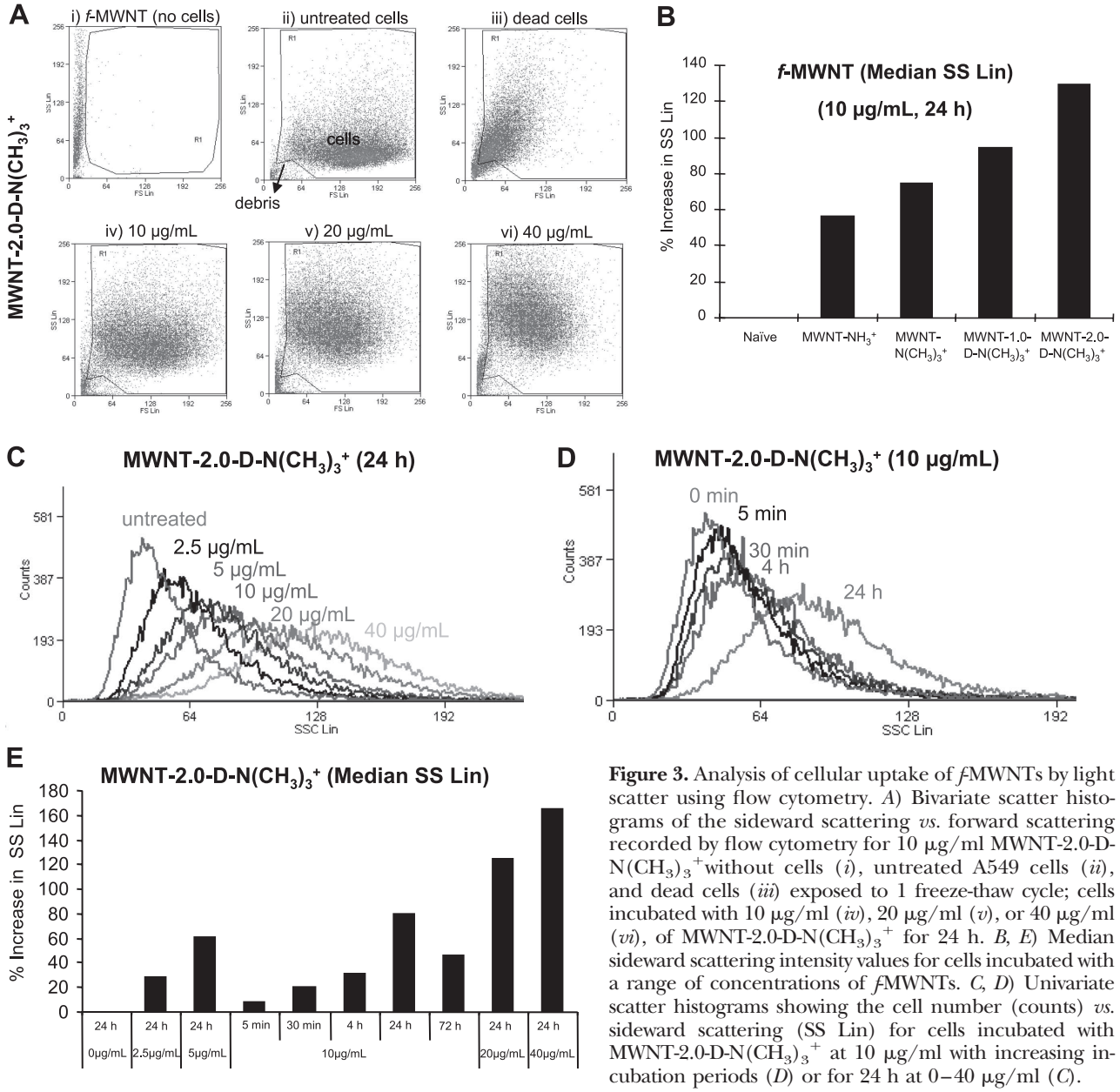

Figure 3. Analysis of cellular uptake of *f*-MWNTs by light scatter using flow cytometry. *A*) Bivariate scatter histograms of the sideward scattering *vs.* forward scattering recorded by flow cytometry for 10 µg/ml MWNT-2.0-D-$N(CH_3)_3^+$without cells (*i*), untreated A549 cells (*ii*), and dead cells (*iii*) exposed to 1 freeze-thaw cycle; cells incubated with 10 µg/ml (*iv*), 20 µg/ml (*v*), or 40 µg/ml (*vi*), of MWNT-2.0-D-$N(CH_3)_3^+$ for 24 h. *B*, *E*) Median sideward scattering intensity values for cells incubated with a range of concentrations of *f*-MWNTs. *C*, *D*) Univariate scatter histograms showing the cell number (counts) *vs.* sideward scattering (SS Lin) for cells incubated with MWNT-2.0-D-$N(CH_3)_3^+$ at 10 µg/ml with increasing incubation periods (*D*) or for 24 h at 0–40 µg/ml (*C*).

ratio. The interaction between siRNA and the MWNT-2.0-D-$N(CH_3)_3^+$ was also shown for the 1:8 and 1:16 mass ratios by TEM (Fig. 5*B*), as evidenced by the formation of areas of high contrast (dark) around the MWNT-2.0-D-$N(CH_3)_3^+$. AFM imaging on mica (in vacuum) of MWNT-2.0-D-$N(CH_3)_3^+$ alone and MWNT-2.0-D-$N(CH_3)_3^+$:siRNA complexes at 1:8 and 1:16 mass ratios was also performed. High magnification AFM images (amplitude and 3-D; Fig. 5*B* and Supplemental Fig. S2) showed that the *f*-MWNT surface was coated by a layer of siRNA, confirming the surface interactions between the 2 oppositely charged components. Cryo-TEM further confirmed the individualization of MWNT-2.0-D-$N(CH_3)_3^+$ even after siRNA complexation (Supplemental Fig. S2).

Uptake of a noncoding siRNA sequence (siNEG) complexed with dendron-MWNTs in A549 was studied at 16:1 mass ratio (final dendron-MWNTs concentration of 16 µg/ml) after 24 h incubation. Optical microscopy of the cell cultures **(Fig. 6*A*)** showed that both the dendron-MWNT alone and the complexes with siRNA were able to internalize into the cytoplasm. We then performed flow cytometry (light scattering by cells) of the A549 cells after incubation with the *f*-MWNT:siRNA complexes to observe a marked shift in sideward scattering, similar to that obtained after incubation with the *f*-MWNT alone (Fig. 6*B*). This indicated that complexation with siRNA did not compromise *f*-MWNT uptake into the cells. To determine whether the siRNA was also internalized, a fluorescently labeled siRNA was used (ATTO 655 probe emitting at λ_{em}=684 nm was conjugated to the 3′ end of the nucleic acid duplex). The ATTO 655-siRNA was complexed with the different *f*-MWNTs and incubated with HeLa cells for 4 and 24 h. For comparison, cationic liposomes (DOTAP:cholesterol) were used. CLSM illustrated a sharp

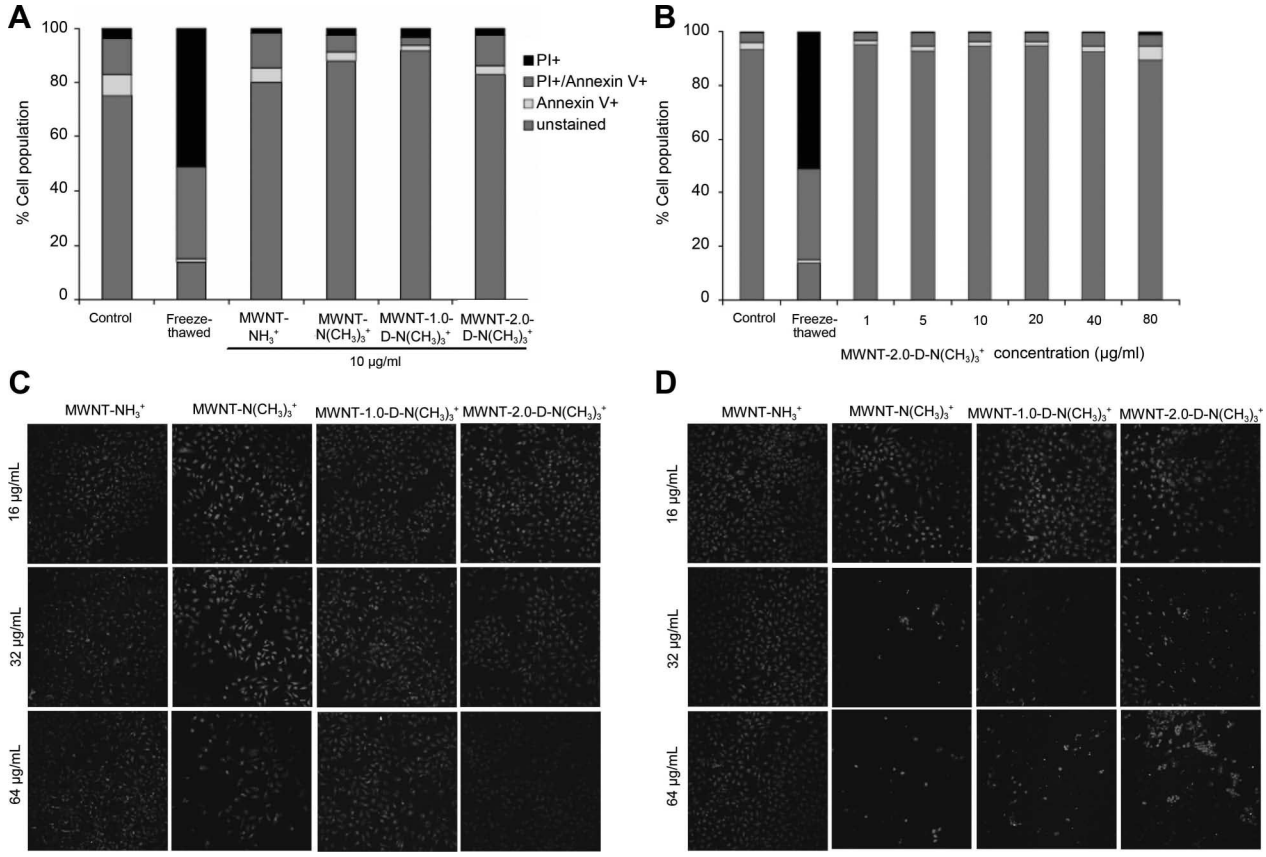

Figure 4. Cell viability of human lung carcinoma A549 cells after 24 h incubation with *f*-MWNTs. *A*, *B*) Percentage viability of A549 assessed by annexin V-FITC/PI staining and quantified by FACS after incubation with *f*-MWNTs at 10 μg/ml final concentration (*A*) or with MWNT-2.0-D-N$(CH_3)_3^+$ at 0–80 μg/ml final concentrations (*B*). *C*, *D*) Cell viability of human cervical cancer cell line HeLa after incubation with *f*-MWNTs by TUNEL labeling. Confocal microscopy images of HeLa cells obtained 24 h (*C*) and 48 h (*D*) after incubation with *f*-MWNTs at 16, 32, and 64 μg/ml final *f*-MWNT concentrations. There was no sign of apoptosis (green fluorescence) seen except after 48 h incubation at 32 and 64 μg/ml *f*-MWNT final concentrations.

difference in the intracellular fluorescence signals obtained with liposome:ATTO 655-siRNA compared with *f*-MWNT:complexes (Fig. 6*C*). The siRNA signal (blue channel) was diffused throughout the cytoplasm of cells treated only with *f*-MWNT:ATTO 655-siRNA complexes (Fig. 6*C*) (32). The more punctate fluorescence signal pattern using liposome:siRNA complexes indicated localization within cellular compartments (*e.g.*, endosomes) and suggested that the mechanism of uptake of siRNA complexed with *f*-MWNT and cationic liposomes was not identical. We further determined that increased degree of dendron branching on the nanotube surface, as in the case of MWNT-1.0-D-N$(CH_3)_3^+$ and MWNT-2.0-D-N$(CH_3)_3^+$, led to significantly enhanced intracellular internalization of the siRNA compared with MWNT-NH_3^+ and MWNT-N$(CH_3)_3^+$.

The ability of *f*-MWNTs to deliver biologically functional siRNA was studied using 2 experimental conditions that evaluated gene silencing activity. First, A549 cells were transfected with siGFP (siRNA silencing the GFP) using cationic liposome:siGFP (positive control) or MWNT-2.0-D-N$(CH_3)_3^+$:siGFP complexes 14 h before an adenovirus (Ad.CMV.GFP) infection that introduces strong GFP expression. **Figure 7*A*** shows semi-quantitatively Western blot data for GFP and GAPDH (housekeeping gene) indicating that MWNT-2.0-D-N$(CH_3)_3^+$ was effective in silencing GFP expression in A549 cells at both 1:8 and 1:16 mass ratios. The equivalent concentration of a scrambled siRNA sequence (siNEG) had almost no effect on GFP expression for both the liposome and CNT vectors. These results indicated that biologically active siGFP could be effectively delivered intracellularly by the dendron-MWNTs.

Further, a different type of siRNA, the commercially available apoptosis-inducing siRNA sequence (siTOX), was used. The terminal TUNEL reaction was used to detect apoptotic cells by fluorescence microscopy. HeLa cells (human cervical carcinoma) were incubated with free siTOX (80 nM) or complexed with all 4 *f*-MWNTs at 1:16 mass ratio (equivalent to 16 μg/ml dendron-MWNT) for 24 h, and apoptosis was assessed after 48 h. HeLa cells were chosen as they were previously screened and found sensitive to siTOX (30). Most cells in the transfected cultures were found apoptotic after 48 h of incubation with the siTOX complexed with MWNT-N$(CH_3)_3^+$, MWNT-1.0-D-N$(CH_3)_3^+$, or MWNT-2.0-D-N$(CH_3)_3^+$ (Fig. 7*B*). Equivalent concentrations of the siTOX (data not shown) or *f*-MWNTs alone (without siTOX complexation) did not lead to apoptosis (Fig. 7*B* and Supplemen-

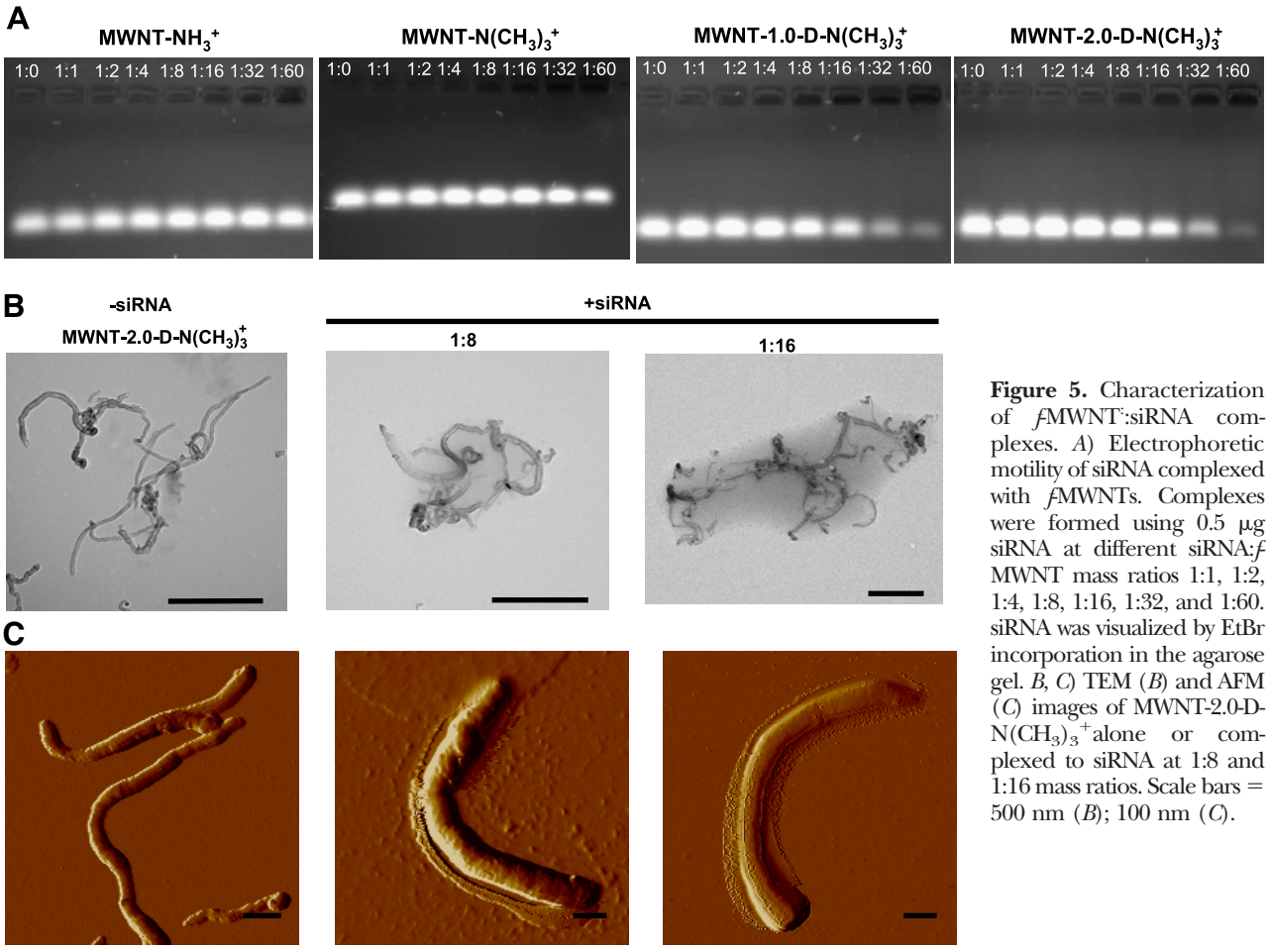

Figure 5. Characterization of *f*MWNT:siRNA complexes. *A*) Electrophoretic motility of siRNA complexed with *f*MWNTs. Complexes were formed using 0.5 μg siRNA at different siRNA:*f*MWNT mass ratios 1:1, 1:2, 1:4, 1:8, 1:16, 1:32, and 1:60. siRNA was visualized by EtBr incorporation in the agarose gel. *B, C*) TEM (*B*) and AFM (*C*) images of MWNT-2.0-D-$N(CH_3)_3^+$alone or complexed to siRNA at 1:8 and 1:16 mass ratios. Scale bars = 500 nm (*B*); 100 nm (*C*).

tal Fig. S3). Overall, these studies indicated that alkylated dendron-MWNTs were able to condense, intracellularly translocate, and successfully deliver biologically active siRNA sequences in a more efficient way than *f*MWNTs with a primary amino group and equivalent to established transfection agents (such as cationic liposomes).

DISCUSSION

In this work, we hypothesized that molecular engineering of functionalized groups on the *f*CNT surface by alkylation of the terminal amino groups and by increasing the degree of dendritic branching could improve water dispersibility and cellular internalization of the nanotubes within mammalian cells. Alkylation of the amino groups on the *f*MWNT surface achieves pH-independent ionization, therefore increased electrostatic repulsion among nanotubes leading to more individually dispersed nanotube in water. Moreover, the enhanced positive charge on the individualized *f*MWNTs could offer stronger electrostatic interactions at physiological pH with the negatively charged cell membrane and negatively charged biomacromolecules (such as pDNA and siRNA).

To increase the degree of polymer branching at the CNT surface in a more precise manner, we used a dendron divergent synthesis approach. Lower generation dendrons were preferred over higher generations in an attempt to maintain the capability of CNTs to interact with biological membranes and minimize cytotoxicity due to excessive positive surface charge (38). As the conjugates of this study are not fluorescently labeled, the cellular uptake was compared on the basis of changes in sideward scattering of the cells before and after incubation with increasing concentrations of nanotubes, in conjunction with optical microscopy of the cell cultures. We observed that alkylation of the terminal amino groups on *f*MWNTs [MWNT-$N(CH_3)_3^+$] improved both the dispersibility and cellular uptake of the construct compared with MWNT-NH_3^+. Indeed, this was demonstrated by the 2-fold increase in the sideward scattering signals of cells treated with MWNT-$N(CH_3)_3^+$ compared with untreated cells, while cells treated with MWNT-NH_3^+ showed only 1-fold increase (Fig. 3*B*). Cellular internalization of the *f*MWNTs was shown by perinuclear accumulation of the gray-colored material by optical microscopy. Overall, the MWNT-2.0-D-$N(CH_3)_3^+$ consistently offered the highest cell internalization compared with the rest of the constructs in the series.

Several *in vitro* cytotoxicity assays have been described in the literature to evaluate the cytotoxicity of CNTs (39, 40) including direct counting of cell num-

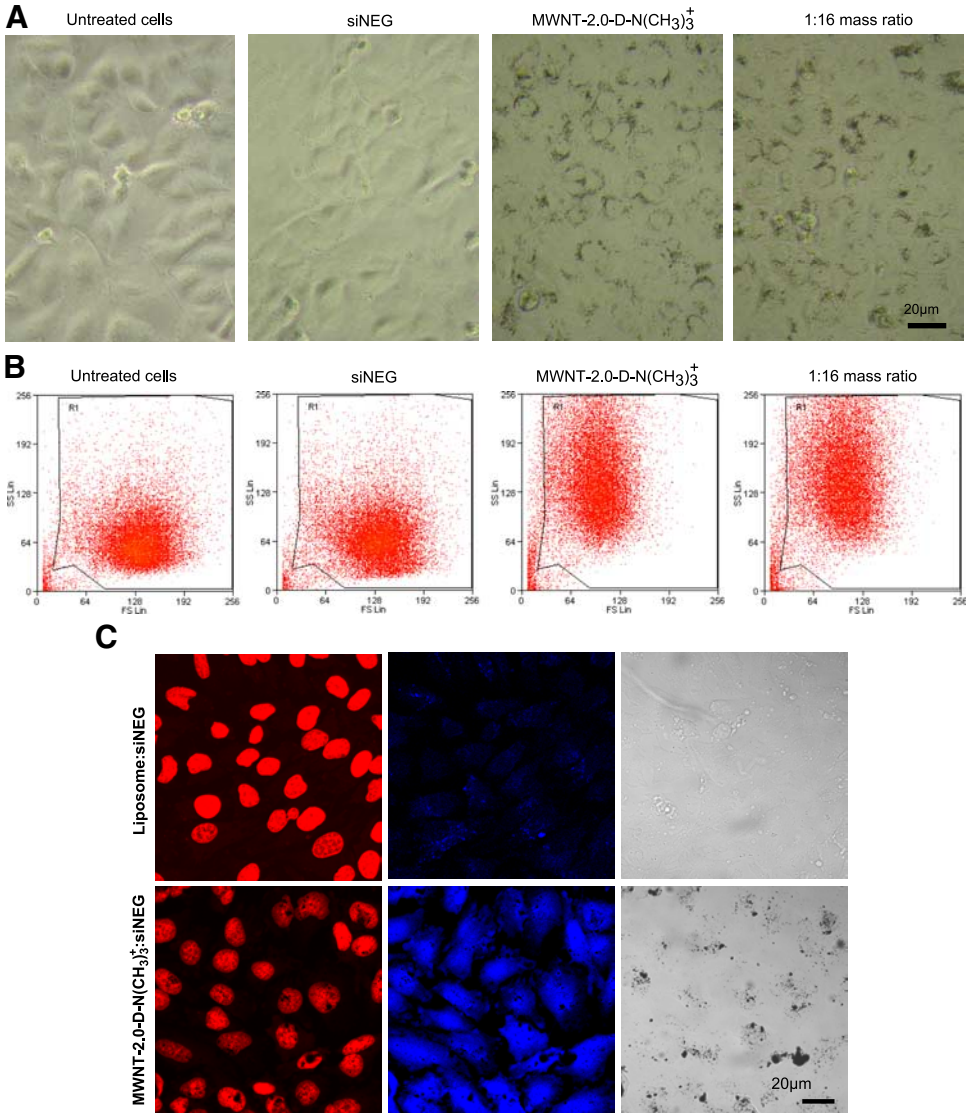

Figure 6. Analysis of cellular uptake of *f*MWNT:siNEG complexes. *A*, *B*) Photomicrographs (*A*) and bivariate scatter histograms (*B*) of control HeLa cells or cells incubated with medium containing 80 nM siNEG, 16 μg/ml MWNT-2.0-D-N$(CH_3)_3^+$, or siNEG: MWNT-2.0-D-N$(CH_3)_3^+$ (1:16) for 24 h. *C*) CLSM images of HeLa cells obtained 24 h after incubation with Atto 655-labeled siRNA: liposome at 1:4 −/+ charge ratio (top panel) or siRNA:MWNT-2.0-D-N$(CH_3)_3^+$ at 1:16 mass ratio equivalent to 16 μg/ml *f*MWNTs (bottom panel), at 80 nM final siRNA concentration. Nuclei were counterstained with PI (red). siRNA intracellular uptake is shown as an increase in blue fluorescence. Images were captured using ×63 lens.

bers by the trypan blue exclusion assay (41), colorimetric assays such as the MTT (42, 43) and LDH assays (43), measurement of protein concentrations by the Bradford assay (44), or clonogenic assays (45). Nevertheless, some studies (43) have shown contradicting cytotoxicity results for CNTs using colorimetry-based assays such as MTT, WST-1, XTT, or LDH with reportedly frequent occurrence of false positive signals. On the other hand, assessing cytotoxicity by flow cytometry can underestimate the extent of cell death since the nature of the experimental conditions may involve removal of dying cells during trypsinization and subsequent rinsing (46). Therefore, herein we considered it prudent to combine the more sensitive fluorescence-based annexin V/PI assay using flow cytometry with the fluorescence microscopy-based TUNEL labeling assay. Concentrations >32 μg/ml induced toxicity in HeLa cells after 48 h incubation as shown by TUNEL labeling (Fig. 4*E*), so investigations in different cell lines using >1 cytotoxicity assay are deemed essential for a comparative toxicological examination of different CNT constructs in general. Thereof, the results generated from 2 different cytotoxic assays in this study indicated that dendron-MWNTs were nontoxic to cells up to concentrations of 80 μg/ml for a maximum exposure time of 24 h. These conditions were further used to assess the biological activity capabilities of the dendron-MWNT series.

Interestingly, increasing the branching of the dendritic component on the nanotubes enhanced their capacity to complex the same amount of siRNA (Fig. 5*A*). The enhanced siRNA complexation was attributed to the increased amount of the cationic charges on the surface of nanotube material in addition to the enhanced dispersibility of the *f*MWNT that increased the total surface area available for siRNA binding. Thus, our results are in complete agreement with what has been previously reported by Krajcik *et al.* (20). In this study, the authors reported that increasing the number of positive charges, wrapping polycationic PDDA onto SWNTs, led to an improvement in both the water dispersibility and siRNA binding.

The type of chemically functionalized MWNTs described here have been designed as biologically rele-

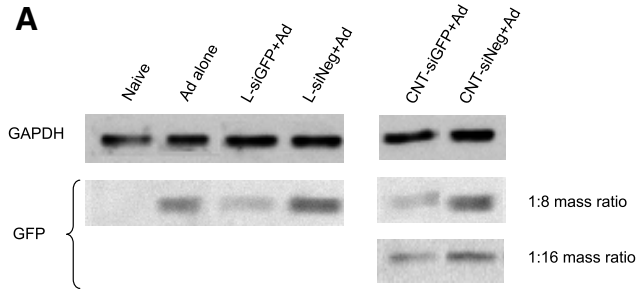

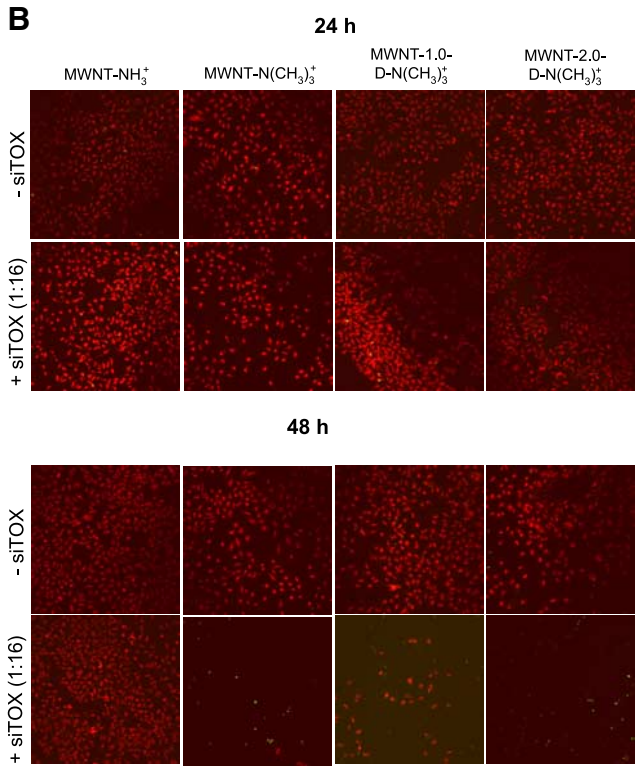

Figure 7. *In vitro* silencing of A549 and HeLa cells. *A*) Western blot of A549 cells 24 h post-transfection with Ad-eGFP (1×10^8 particles/well); monolayers were pretreated (14 h prior viral transfection) with either siGFP: cationic liposome or siGFP:MWNT-2.0-D-N$(CH_3)_3^+$ complexes at 52 nM siGFP final concentration. Preincubation of the cells with siGFP complexes led to a reduction in eGFP expression at both 1:8 and 1:16 mass ratios. GAPDH was used as an internal standard. *B*) CLSM images of HeLa cells showing TUNEL labeling after transfection with siTOX:*f*MWNT complexes at 1:16 mass ratio and 80 nM final siTOX concentration for 24 or 48 h. Only cells treated with siTOX complexed with the MWNT-N$(CH_3)_3^+$, MWNT-1.0-D-N$(CH_3)_3^+$, and MWNT-2.0-D-N$(CH_3)_3^+$ showed green fluorescence (apoptosis) 48 h post-transfection. Images were captured using ×10 lens.

vant dendron-MWNT constructs with a precisely tailored number of polycationic functional groups that can internalize into mammalian cells effectively with minimal induced cytotoxicity. Moreover, these dendron-MWNT constructs have been shown to complex negatively charged double-stranded siRNA and mediate its efficient intracellular delivery and biological activity constituting them as promising candidate vectors for *in vivo* gene silencing. FJ

This work was supported by the University of Trieste; Italian Ministry of Education MUR (cofin Prot. 2006034372 and Firb RBIN04HC3S); Regione Friuli Venezia-Giulia; The School of Pharmacy, University of London; CNRS; and Agence Nationale de la Recherche (grant ANR-05-JCJC-0031-01). Partial support is also acknowledged by the European Union FP6 NEURONANO (NMP4-CT-2006-031847), NINIVE (NMP4-CT-2006-033378) and FP7 ANTICARB (HEALTH-2007-201587) programs. M.A.H. acknowledges support by the Junta de Comunidades de Castilla la Mancha (Spain) for the award of a postdoctoral fellowship.

REFERENCES

1. Bianco, A., Kostarelos, K., and Prato, M. (2005) Applications of carbon nanotubes in drug delivery. *Curr. Opin. Chem. Biol.* **9,** 674–679
2. Bianco, A., Kostarelos, K., and Prato, M. (2008) Opportunities and challenges of carbon-based nanomaterials for cancer therapy. *Expert Opin. Drug Deliv.* **5,** 331–342
3. Lacerda, L., Bianco, A., Prato, M., and Kostarelos, K. (2006) Carbon nanotubes as nanomedicines: from toxicology to pharmacology. *Adv. Drug Deliv. Rev.* **58,** 1460–1470
4. Kostarelos, K., Lacerda, L., Pastorin, G., Wu, W., Wieckowski, S., Luangsivilay, J., Godefroy, S., Pantarotto, D., Briand, J. P., Muller, S., Prato, M., and Bianco, A. (2007) Cellular uptake of functionalized carbon nanotubes is independent of functional group and cell type. *Nat. Nanotechnol.* **2,** 108–113
5. Becker, M. L., Fagan, J. A., Gallant, N. D., Bauer, B. J., Bajpai, V., Hobbie, E. K., Lacerda, S. H., Migler, K. B., and Jakupciak, J. P. (2007) Length-dependent uptake of DNA-wrapped single-walled carbon nanotubes. *Adv. Mat.* **19,** 939–945
6. Kam, N. W. S., Jessop, T. C., Wender, P. A., and Dai, H. J. (2004) Nanotube molecular transporters: internalization of carbon nanotube-protein conjugates into mammalian cells. *J. Am. Chem. Soc.* **126,** 6850–6851
7. Kam, N. W. S., Liu, Z. A., and Dai, H. J. (2006) Carbon nanotubes as intracellular transporters for proteins and DNA: An investigation of the uptake mechanism and pathway. *Angew. Chem. Int. Ed.* **45,** 577–581
8. Kang, B., Yu, D. C., Chang, S. Q., Chen, D., Dai, Y. D., and Ding, Y. T. (2008) Intracellular uptake, trafficking and subcellular distribution of folate conjugated single walled carbon nanotubes within living cells. *Nanotechnology* **19,** 375103–375111
9. Ali-Boucetta, H., Al-Jamal, K. T., McCarthy, D., Prato, M., Bianco, A., and Kostarelos, K. (2008) Multiwalled carbon nanotube-doxorubicin supramolecular complexes for cancer therapeutics. *Chem. Commun. (Camb.)* 459–461
10. Chen, J., Chen, S., Zhao, X., Kuznetsova, L. V., Wong, S. S., and Ojima, I. (2008) Functionalized single-walled carbon nanotubes as rationally designed vehicles for tumor-targeted drug delivery. *J. Am. Chem. Soc.* **130,** 16785
11. Hampel, S., Kunze, D., Haase, D., Kramer, K., Rauschenbach, M., Ritschel, M., Leonhardt, A., Thomas, J., Oswald, S., Hoffmann, V., and Buchner, B. (2008) Carbon nanotubes filled with a chemotherapeutic agent: a nanocarrier mediates inhibition of tumor cell growth. *Nanomedicine* **3,** 175–182
12. Liu, Z., Chen, K., Davis, C., Sherlock, S., Cao, Q., Chen, X., and Dai, H. (2008) Drug delivery with carbon nanotubes for in vivo cancer treatment. *Cancer Res.* **68,** 6652–6660
13. Wu, W., Wieckowski, S., Pastorin, G., Benincasa, M., Klumpp, C., Briand, J. P., Gennaro, R., Prato, M., and Bianco, A. (2005) Targeted delivery of amphotericin B to cells by using functionalized carbon nanotubes. *Angew. Chem. Int. Ed. Engl.* **44,** 6358–6362
14. Bianco, A., Hoebeke, J., Godefroy, S., Chaloin, O., Pantarotto, D., Briand, J. P., Muller, S., Prato, M., and Partidos, C. D. (2005)

Cationic carbon nanotubes bind to CpG oligodeoxynucleotides and enhance their immunostimulatory properties. *J. Am. Chem. Soc.* **127,** 58–59
15. Kam, N. W. S., and Dai, H. J. (2005) Carbon nanotubes as intracellular protein transporters: Generality and biological functionality. *J. Am. Chem. Soc.* **127,** 6021–6026
16. Pantarotto, D., Briand, J. P., Prato, M., and Bianco, A. (2004) Translocation of bioactive peptides across cell membranes by carbon nanotubes. *Chem. Commun.* 16–17
17. Yu, B. Z., Yang, J. S., and Li, W. X. (2007) In vitro capability of multi-walled carbon nanotubes modified with gonadotrophin releasing hormone on killing cancer cells. *Carbon* **45,** 1921–1927
18. Kam, N. W., Liu, Z., and Dai, H. (2005) Functionalization of carbon nanotubes via cleavable disulfide bonds for efficient intracellular delivery of siRNA and potent gene silencing. *J. Am. Chem. Soc.* **127,** 12492–12493
19. Kateb, B., Van, H. M., Zhang, L., Bronikowski, M. J., Manohara, H., and Badie, B. (2007) Internalization of MWCNTs by microglia: possible application in immunotherapy of brain tumors. *Neuroimage* **37**(Suppl. 1), S9–S17
20. Krajcik, R., Jung, A., Hirsch, A., Neuhuber, W., and Zolk, O. (2008) Functionalization of carbon nanotubes enables noncovalent binding and intracellular delivery of small interfering RNA for efficient knock-down of genes. *Biochem. Biophys. Res. Commun.* **369,** 595–602
21. Lanner, J. T., Bruton, J. D., ssefaw-Redda, Y., Andronache, Z., Zhang, S. J., Severa, D., Zhang, Z. B., Melzer, W., Zhang, S. L., Katz, A., and Westerblad, H. (2009) Knockdown of TRPC3 with siRNA coupled to carbon nanotubes results in decreased insulin-mediated glucose uptake in adult skeletal muscle cells. *FASEB J.* **23,** 1728–1738
22. Liu, Z., Winters, M., Holodniy, M., and Dai, H. (2007) siRNA delivery into human T cells and primary cells with carbon-nanotube transporters. *Angew. Chem. Int. Ed. Engl.* **46,** 2023–2027
23. Zhang, Z., Yang, X., Zhang, Y., Zeng, B., Wang, S., Zhu, T., Roden, R. B., Chen, Y., and Yang, R. (2006) Delivery of telomerase reverse transcriptase small interfering RNA in complex with positively charged single-walled carbon nanotubes suppresses tumor growth. *Clin. Cancer Res.* **12,** 4933–4939
24. Gao, L., Nie, L., Wang, T., Qin, Y., Guo, Z., Yang, D., and Yan, X. (2006) Carbon nanotube delivery of the GFP gene into mammalian cells. *Chembiochemical* **7,** 239–242
25. Liu, Y., Wu, D. C., Zhang, W. D., Jiang, X., He, C. B., Chung, T. S., Goh, S. H., and Leong, K. W. (2005) Polyethyleniminegrafted multiwalled carbon nanotubes for secure noncovalent immobilization and efficient delivery of DNA. *Angew. Chem. Int. Ed.*. **44,** 4782–4785
26. Pantarotto, D., Singh, R., McCarthy, D., Erhardt, M., Briand, J. P., Prato, M., Kostarelos, K., Bianco, A. (2004) Functionalized carbon nanotubes for plasmid DNA gene delivery. *Angew. Chem. Int. Ed.* **43,** 5242–5246
27. Singh, R., Pantarotto, D., McCarthy, D., Chaloin, O., Hoebeke, J., Partidos, C. D., Briand, J. P., Prato, M., Bianco, A., and Kostarelos, K. (2005) Binding and condensation of plasmid DNA onto functionalized carbon nanotubes: Toward the construction of nanotube-based gene delivery vectors. *J. Am. Chem. Soc.* **127,** 4388–4396
28. Bianco, A., Kostarelos, K., Partidos, C. D., and Prato, M. (2005) Biomedical applications of functionalised carbon nanotubes. *Chem. Comm.* 571–577
29. Wang, X., Ren, J., and Qu, X. (2008) Targeted RNA interference of cyclin A2 mediated by functionalized single-walled carbon nanotubes induces proliferation arrest and apoptosis in chronic myelogenous leukemia K562 cells. *Chem. Med. Chem.* **3,** 940–945
30. Podesta, J. E., Al-Jamal, K. T., Herrero, M. A., Tian, B., li-Boucetta, H., Hegde, V., Bianco, A., Prato, M., and Kostarelos, K. (2009) Antitumor activity and prolonged survival by carbon-nanotube-mediated therapeutic siRNA silencing in a human lung xenograft model. *Small* **5,** 1176–1185
31. Campidelli, S., Sooambar, C., Lozano, D. E., Ehli, C., Guldi, D. M., and Prato, M. (2006) Dendrimer-functionalized single-wall carbon nanotubes: synthesis, characterization, and photoinduced electron transfer. *J. Am. Chem. Soc.* **128,** 12544–12552
32. Herrero, M. A., Toma, F. M., Al-Jamal, K. T., Kostarelos, K., Bianco, A., Da, R. T., Bano, F., Casalis, L., Scoles, G., and Prato, M. (2009) Synthesis and characterization of a carbon nanotube-dendron series for efficient siRNA delivery. *J. Am. Chem. Soc.* **131,** 9843–9848
33. Lacerda, L., Raffa, S., Prato, M., Bianco, A., and Kostarelos, K. (2007) Cell-penetrating CNTs for delivery of therapeutics. *Nano Today* **2,** 38–43
34. Lacerda, L., Pastorin, G., Gathercole, D., Buddle, J., Prato, M., Bianco, A., and Kostarelos, K. (2007) Intracellular trafficking of carbon nanotubes by confocal laser scanning microscopy. *Adv. Mat.* **19,** 1480–1484
35. Cai, D., Blair, D., Dufort, F. J., Gumina, M. R., Huang, Z., Hong, G., Wagner, D., Canahan, D., Kempa, K., Ren, Z. F., and Chiles, T. C. (2008) Interaction between carbon nanotubes and mammalian cells; characterization by flow cytometry and application. *Nanotechnology* **19,** 1–10
36. Compton, M. M. (1992) A biochemical hallmark of apoptosis: internucleosomal degradation of the genome. *Cancer Metastasis Rev.* **11,** 105–119
37. Dive, C., Gregory, C. D., Phipps, D. J., Evans, D. L., Milner, A. E., and Wyllie, A. H. (1992) Analysis and discrimination of necrosis and apoptosis (programmed cell death) by multiparameter flow cytometry. *Biochim. Biophys. Acta* **1133,** 275–285
38. Jevprasesphant, R., Penny, J., Jalal, R., Attwood, D., McKeown, N. B., and D'Emanuele, A. (2003) The influence of surface modification on the cytotoxicity of PAMAM dendrimers. *Int. J. Pharm.* **252,** 263–266
39. Smart, S. K., Cassady, A. I., Lu, G. Q., and Martin, D. J. (2006) The biocompatibility of carbon nanotubes. *Carbon* **44,** 1034–1047
40. Ying, Z., WenXin, L. (2008) Cytotoxicity of carbon nanotubes. *Sci. China Ser. B-Chem.* **51,** 1021–1029
41. Bottini, M., Bruckner, S., Nika, K., Bottini, N., Bellucci, S., Magrini, A., Bergamaschi, A., and Mustelin, T. (2006) Multi-walled carbon nanotubes induce T lymphocyte apoptosis. *Toxicol. Lett.* **160,** 121–126
42. Davoren, M., Herzog, E., Casey, A., Cottineau, B., Chambers, G., Byrne, H. J., and Lyng, F. M. (2007) In vitro toxicity evaluation of single walled carbon nanotubes on human A549 lung cells. *Toxicol. In Vitro* **21,** 438–448
43. Worle-Knirsch, J. M., Pulskamp, K., and Krug, H. F. (2006) Oops they did it again! Carbon nanotubes hoax scientists in viability assays. *Nano Lett.* **6,** 1261–1268
44. Isobe, H., Tanaka, T., Maeda, R., Noiri, E., Solin, N., Yudasaka, M., Iijima, S., and Nakamura, E. (2006) Preparation, purification, characterization, and cytotoxicity assessment of water-soluble, transition-metal-free carbon nanotube aggregates. *Angew. Chem. Int. Ed. Engl.* **45,** 6676–6680
45. Herzog, E., Casey, A., Lyng, F. M., Chambers, G., Byrne, H. J., and Davoren, M. (2007) A new approach to the toxicity testing of carbon-based nanomaterials–the clonogenic assay. *Toxicol. Lett.* **174,** 49–60
46. Monteiro-Riviere, N. A., Inman, A. O., and Zhang, L. W. (2009) Limitations and relative utility of screening assays to assess engineered nanoparticle toxicity in a human cell line. *Toxicol. Appl. Pharmacol.* **234,** 222–235

Received for publication March 15, 2010.
Accepted for publication June 24, 2010.